V. CASTELLI
Columbia University,
New York, N. Y., and
Franklin Institute Research Laboratories,
Philadelphia, Pa.

J. T. McCABE
Franklin Institute Research Laboratories,
Philadelphia, Pa.
Assoc. Mem. ASME

Transient Dynamics of a Tilting Pad Gas Bearing System

A method for obtaining the performance characteristics of a rotor-tilting pad gas lubricated journal bearing system by solving the appropriate dynamics equations together with the time-transient Reynolds' equation is outlined. Results for a 4 degree of freedom and an 18 degree of freedom system are given. Comparison with steady-state and experimental results are also discussed.

Introduction

THE WORK presented in this paper was motivated by the necessity of evaluating performance characteristics of a space power rotor system. Many design considerations, among which are self-alignment and excellent probability of stable operation, dictated the selection of tilting pad bearings. After the basic design was established from steady-state analysis of the load capacity, power loss, minimum clearance, and thermal transient, a need was felt for an investigation of the complete system dynamics.

The configuration under study contained a rigid rotor supported by two bearings with three pivoted shoes each. One of the shoes on each bearing was riding a spring-loaded pivot. (Some results are also given for the dynamical characteristics of a shaft and a single-pivoted pad bearing.)

Neglecting the yaw of each pad, eighteen degrees of freedom were necessary to describe the motion: Two translations and two tilts for the shaft, roll and pitch of each shoe, and translation of two pivots along pivot axis.

The bearing forces in each pad were evaluated by integration of the lubrication equation with full account of geometrical and pressure transient terms. The forces were used in the dynamic equations for all degrees of freedom involved. The entire time history of the motion of each part of the system subsequent to arbitrary initial conditions was obtained and examined for stability, frequency response, steady-state characteristics, and sensitivity to unbalance.

The detailed treatment of both the lubrication equation and the system dynamics is presented in the following since it can be of interest for related studies.

Contributed by the Lubrication Division and presented at the Lubrication Symposium, New Orleans, La., June 5–9, 1966, of THE AMERICAN SOCIETY OF MECHANICAL ENGINEERS. Manuscript received at ASME Headquarters, March 10, 1966. Paper No. 66—LubS-3.

Dynamics

Shaft Dynamics

The shaft is assumed to be a rigid body and its motion identified with the motion of the geometrical axis. The kinematic parameters involved are shown in Fig. 1. A reference stationary coordinate system is selected so that the x-y plane contains the shaft mass center. The thrust bearings restraining the axial motion of the shaft are assumed to exist but are not considered in the system. In the present system the unbalance is considered as an external load caused by a point mass (m_2) attached to the surface of the shaft in the cross-sectional plane containing the center of mass, and two equal masses (m_1) attached to the surface of the shaft each at a distance ρ_u from the aforementioned plane and located symmetrically with respect to the mass center. Upon rotation a force $\mathbf{F}_u$ and a moment $\mathbf{M}_u$ at the mass center are generated (Fig. 2) which revolve synchronously with the shaft. The magnitudes of the unbalance force and moment are

$$|\mathbf{F}_u| = Rm_2\Omega^2 \tag{1}$$

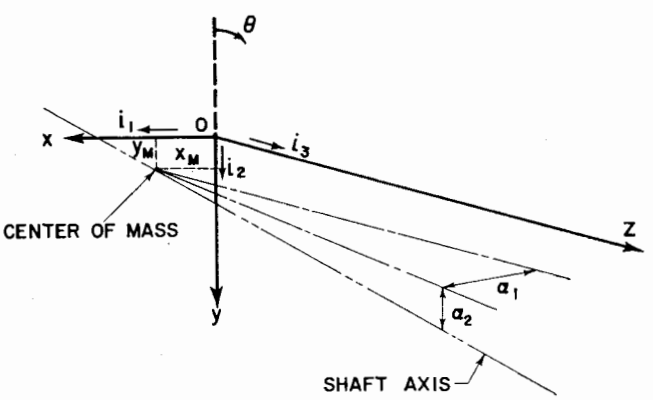

Fig. 1 Journal coordinate system

Nomenclature

$A_1 = \alpha_1 L/c$

$A_2 = \alpha_2 L/c$

$B = \dfrac{p_a RL}{mc\,(\Omega/2)^2}$

c = radius of shoe—radius of shaft

c' = radius of pivot circle—radius of shaft

$D = d/R$

d = distance from face of shoe to pivot point

$\mathbf{F}_u$ = unbalance force = $Rm_2\Omega^2$

$G = 2I_p/I_t$

I_p, I_t = shaft polar and transverse moments of inertia

I_{11}', I_{22}' = shoe pitch and roll moments of inertia

$I = \dfrac{p_a RL^3}{I_t c(\Omega/2)^2}$

$I_\Delta = \dfrac{p_a R^2 L}{(I_{11}' - m'\rho_{O2})} \times (R/c)(2/\Omega)^2$

$I_\Gamma = \dfrac{p_a RL^2}{I_{22}'} \times (L/c)(2/\Omega)^2$

$K = kc/p_a RL$

L = axial width of shoe

k = preload spring constant

$\mathbf{M}_u$ = unbalance moment = $2m_1 R$-$\rho_u\Omega^2$

m = shaft mass

m' = mass of shoe

m_1, m_2 = shaft unbalance masses

θ = angular coordinates measured from $-y$ axis in the direction of shaft rotation

θ_p = θ at a pivot

$P = p/p_a$ {p_a = ambient pressure}

(Continued on next page)

$$|\mathbf{M}_u| = 2m_1R\rho_u\Omega^2 \tag{2}$$

The angle between $\mathbf{F}_u$ and $\mathbf{M}_u$ is called ϕ_u.

The translational motion of the center of mass is governed by the equation

$$m\frac{d^2}{dt}\mathring{\mathbf{r}}_m = \mathbf{f} \tag{3}$$

where $\mathring{\mathbf{r}}_m = x_m\mathbf{i} + y_m\mathbf{j}$ the two-dimensional vector position of the shaft mass center and $\mathbf{f}$ is defined as

$$\mathbf{f} = f_x\mathbf{i} + f_y\mathbf{j}$$

$$f\begin{Bmatrix} x \\ y \end{Bmatrix} = \sum_{k=1}^{n_p}\iint_{s\ k}(p - p_a)\begin{Bmatrix}\sin\theta \\ \cos\theta\end{Bmatrix}Rd\theta dz + w\begin{Bmatrix} x \\ y\end{Bmatrix} - m_2R\Omega^2\begin{Bmatrix}\cos\Omega t \\ \sin\Omega t\end{Bmatrix} \tag{4}$$

where n_p = number of bearing pads.

Equation (3) can be made dimensionless by dividing by $mc(\Omega/2)^2$

$$\frac{d^2}{dT^2}\begin{Bmatrix}X_m \\ Y_m\end{Bmatrix} = B\left[\sum_{k=1}^{n_p}\iint_{s\ k}(P-1)\begin{Bmatrix}\sin\theta \\ \cos\theta\end{Bmatrix}d\theta dZ + W\begin{Bmatrix}x \\ y\end{Bmatrix} - U_f\begin{Bmatrix}\sin 2T \\ \cos 2T\end{Bmatrix}\right] \tag{5}$$

The angular motion of the shaft is governed by

$$\frac{d\mathbf{H}}{dt} = \mathbf{M} = \text{total external moment (including unbalance)} \tag{6}$$

where

$\mathbf{H} = I_{ij}\omega_j\mathbf{i}_i$ = angular momentum about center of mass
I_{ij} = inertia tensor about the $\mathbf{i}_i$ axis
$\boldsymbol{\omega}$ = total angular velocity of shaft

If the $\mathbf{i}_3$ axis coincides with the shaft axis

$$\mathring{I}_{ij} = 0 \tag{7}$$

$$I_{ij} = \delta_{ij}I_{(i)} \quad \text{(no sum)}$$
$$I_{(1)} = I_{(2)} = I_t;\ I_{(3)} = I_p \tag{8}$$

where (1), etc., refers to $i = j = 1$, etc.

Selecting the angular velocity of the i_i system to be

$$\chi = \boldsymbol{\omega} - \omega_3\mathbf{i}_3 \tag{9}$$

equation (6) becomes

$$M_1 = I_T\mathring{\omega}_1 + I_p\omega_2\omega_3$$
$$M_2 = I_T\mathring{\omega}_2 - I_p\omega_1\omega_3 \tag{10}$$
$$M_3 = I_p\mathring{\omega}_3$$

Assuming that the axial driving torque is always balanced by friction, windage, and output torque,

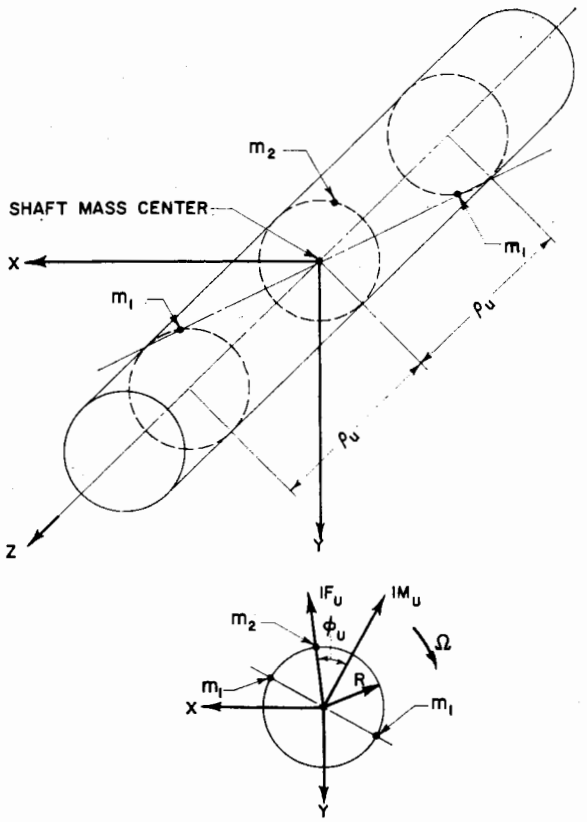

Fig. 2 Unbalance mass system

$$M_3 = 0 \quad \text{and} \quad \omega_3 = \text{const} = -\Omega \tag{11}$$

Due to the smallness of the angles involved, the following expressions can be used for the angular velocity

$$\omega_1 = -\mathring{\alpha}_2;\ \omega_2 = \mathring{\alpha}_1 \tag{12}$$

the moments are

$$\begin{Bmatrix}M_1 \\ M_2\end{Bmatrix} = \begin{Bmatrix}-\\+\end{Bmatrix}\sum_{k=1}^{n_p}\iint_{s\ k}z(p-p_a)\begin{Bmatrix}\cos\theta \\ \sin\theta\end{Bmatrix}Rd\theta dz + M_0\begin{Bmatrix}1 \\ 2\end{Bmatrix} + (2m_1R\rho_u\Omega^2)\begin{Bmatrix}\cos(\Omega t + \phi_u) \\ -\sin(\Omega t + \phi_u)\end{Bmatrix} \tag{13}$$

where the subscripts 1 and 2 refer to the i_1 and i_2 directions. Equation (10) can be made dimensionless by dividing by $I_tc(\Omega/2)^2$:

$$\frac{d^2}{dT^2}\begin{Bmatrix}A_2 \\ A_1\end{Bmatrix} = G\frac{d}{dT}\begin{Bmatrix}-A_1 \\ +A_2\end{Bmatrix} + I\left[\sum_{k=1}^{n_p}\iint_{sk}ZP\begin{Bmatrix}\cos\theta \\ \sin\theta\end{Bmatrix}d\theta dZ + \begin{Bmatrix}-M_{01} \\ +M_{02}\end{Bmatrix} + U_m\begin{Bmatrix}\sin(2T+\phi_u) \\ -\cos(2T+\phi_u)\end{Bmatrix}\right] \tag{14}$$

Nomenclature

R = radius of shaft
$\mathbf{r}_m$ = position vector of shaft mass center
t = time variable
$T = t\Omega/2$
$X, Y, Z = x/c, y/c, z/L$
w_x, w_y = external loads
$X_1', X_2', X_3' = \frac{x_1'}{c}, \frac{x_2'}{c}, \frac{x_3'}{c}$ shoe coordinates
$\Gamma = \gamma_1L/c$
$\Delta = \delta R/c$
ϵ = shoe-shaft coordinate (eccentricity ratio)
α_1, α_2 = angular coordinates of shaft axis
γ = shoe roll angular coordinate
δ = shoe pitch angular coordinate
ξ = shoe-shaft coordinate (lead angle)
ρ_G = distance from shoe pivot point to shoe mass center
ρ_u = distance from x-y plane to m_1
$\varphi = \theta_p - \theta$
Ω = shaft speed
$\omega_1, \omega_2, \omega_3$ = i_1, i_2, i_3 components of shaft angular velocity
$\omega_1', \omega_2', \omega_3'$ = X_1', X_2', X_3' components of shoe angular velocity

Pad Dynamics

Referring to Fig. 3 the dynamic equations for the motion of each pad are written, relative to the pivotal point 0′

$$\mathbf{F}' = m' \frac{d^2}{dt^2}(\mathbf{R} + \boldsymbol{\rho}_G) \tag{15}$$

$$\bar{\mathbf{T}}_0' = \left(\boldsymbol{\rho}_G \times m' \frac{d^2\mathbf{R}}{dt^2}\right) + \frac{d\mathbf{H}_0'}{dt} \tag{16}$$

The first terms of equations (15) and (16) are equal to zero if the pivot is fixed. Since the pivot points can only move in the X_3'-direction, the use of equation (15) is restricted only to a single component. Expressing the angular velocity of the pad by $\boldsymbol{\omega}'$ the third component of equation (15) becomes

$$m' \frac{d^2R_3}{dt^2} = \iint (p - p_a)\cos\varphi R d\varphi dz + w_3' - k(R_3 - R_0) + m'(\dot{\omega}_1' + \omega_2'\omega_3')\rho_{G2} - m'(\omega_1'^2 + \omega_2'^2)\rho_{G3} \tag{17}$$

where the pad mass center was taken to be on the X_2'–X_3' plane.

In the treatment of equation (16) the axes X_1', X_2', X_3' are initially assigned to move with the pad. Their X_1' axis is a principal axis and the components of dH_0'/dt are

$$1' \text{ comp} = \mathring{\omega}_1' I_{11}' + \omega_2'[\omega_2' I_{32} + \omega_3' I_{33}] - \omega_3'[\omega_2' I_{22} + \omega_3' I_{23}]$$
$$2' \text{ comp} = \mathring{\omega}_2' I_{22}' + \omega_3' I_{23}' + \omega_3' I_{11}'\omega_1' - \omega_1'[I_{32}'\omega_2' + I_{33}'\omega_3']$$
$$3' \text{ comp} = \omega_2' I_{32}' + \mathring{\omega}_3' I_{33}' + \omega_1'[I_{22}'\omega_2' + I_{23}'\omega_3'] - \omega_2'[I_{11}'\omega_1']$$

The first term on the right-hand side of equation (16) contributes only to the X_1' component.

Due to the smallness of the shoe motion it is possible to identify the components along the moving axes with those along the fixed set X_1', X_2', X_3'. Excluding the yaw motion ($\omega_3' = 0$) equation (16) becomes:

$$T_1' - m'\left(\frac{d^2R_3}{dt^2}\right)\rho_{G2} = \mathring{\omega}_1' I_{11}' + \omega_2'^2 I_{32}' \tag{18}$$

$$T_2' = \mathring{\omega}_2' I_{22}' - \omega_1'\omega_2' I_{32}' \tag{19}$$

$$T_3' = \mathring{\omega}_2' I_{32}' + \omega_1'\omega_2'(I_{22}' - I_{11}')$$

The first two equations are used to compute the shaft motion while the third produces the value of the torque necessary to eliminate yaw motion. The torques are given by

$$T_p = \frac{T_1'}{p_a R^2 L} = \iint_s (P - 1)\left(\frac{d}{R} + 1\right)\sin\varphi d\varphi dZ \tag{20}$$

$$T_r = \frac{T_2'}{p_a R L^2} = \iint_s P(Z - Z_B)\cos\varphi d\varphi dZ \tag{21}$$

Neglecting products of angular velocities with respect to their first powers, renaming $\omega_1' = \dot{\delta}$; $\omega_2' = \dot{\gamma}$; $R_3 = x_3'$; eliminating $\ddot{\gamma}$ in equation (17) by using equation (18) and nondimensionalizing

$$\frac{d^2\Delta}{dt^2} = I_\Delta\left[T_p + \left\{W_3' + KC_p + \iint_s (P - 1)\cos\varphi d\varphi dZ\right\}\frac{\rho_{G2}}{R}\right] \tag{22}$$

$$\frac{d^2\Gamma}{dt^2} = I_\Gamma T_r \tag{23}$$

$$\frac{d^2C_p}{dT^2} = I_\Delta\left[\left(W_3' - KC_p + \iint_s (P - 1)\cos\varphi d\varphi dZ\right)\frac{I_{11}'}{m'R^2} - T_p\frac{\rho_{G2}}{R}\right] \tag{24}$$

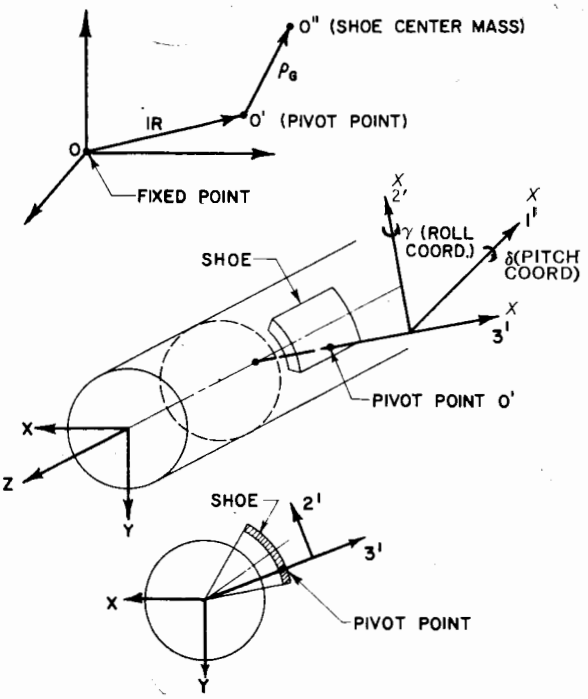

Fig. 3 Shoe coordinate system

Integration Method

The integration of equations (5), (14), (22), (23), and (24) is accomplished in the following manner:

The acceleration $a^{(n)}$ of each degree of freedom is evaluated as the right-hand side of the aforementioned equations at the nth time interval.

The velocity V and position coordinate x are then extrapolated by the formulas

$$V^{(n+1)} = V^{(n)} + a^{(n)} * \Delta T$$
$$X^{(n+1)} = X^{(n)} + V^{(n+1)} * \Delta T$$

The details of such a procedure are discussed in reference [2].

Bearing Film Clearance

To evaluate the film clearance the shaft axis is initially coincident with the z-axis and all shoe bearing surfaces lie on a cylinder of radius $(R + c)$ having z as its axis. The film clearance is now c everywhere. Motions of the shoes and shaft alter the film thickness by the following amounts:

(*a*) translation of shaft; $x_m \sin\theta + y_m \cos\theta$
(*b*) tilting of shaft; $\alpha_1 z \sin\theta + \alpha_2 z \cos\theta$
(*c*) radial translation of shoe; $x_3' \cos\varphi$
(*d*) pitch of shoe; $(d + R\cos\varphi)\delta$
(*e*) roll of shoe; $\gamma(z - z_B)\cos\varphi$

Therefore, the dimensionless film thickness is

$$H = 1 + (X_m + A_1 Z)\sin\theta + (Y_m + A_2 Z)\cos\theta + (D + 1)\Delta\sin\varphi + [(Z - Z_B)\Gamma + X_3']\cos\varphi \tag{25}$$

In equation (25) X_m, A_1, Y_m, A_2, Δ, Γ, and X_3' are functions of time.

In each bearing film the pressure is regulated by the isothermal Reynolds' equation

$$\nabla\cdot(H^3 P \nabla P) = \Lambda\left\{\frac{\partial PH}{\partial\theta} + \frac{\partial PH}{\partial T}\right\} \tag{26}$$

where

$$\nabla = \mathbf{a}\frac{\partial}{\partial\theta} + \mathbf{b}\frac{R}{L}\frac{\partial}{\partial Z}$$

defining $\psi = PH$, equation (26) becomes

$$\nabla^2\psi - \frac{\Lambda}{\psi H}\psi_T = \frac{\Lambda\psi_\theta}{\psi H} - \frac{(\nabla\psi)^2}{\psi} + \frac{\nabla\psi\nabla H}{H} + \frac{\psi}{H}\nabla^2 H \equiv F(\psi, H) \quad (27)$$

To enhance the numerical stability of the integration the following time discretized model is used:

$$\nabla^2\psi^{(n+1)} - \frac{\Lambda\psi^{(n+1)}}{\psi^{(n)}H^{(n)}\Delta T} = \frac{-\Lambda}{H^{(n)}\Delta T} + F(\psi^{(n)}, H^{(n)}) \quad (28)$$

where n, $n+1$ superscripts denote values of the variable at the nth and $(n+1)$th time interval, respectively.

Equation (28) is of the form $\Delta^2\psi(x,y) - f(x,y)\psi(x,y) = g(x,y)$ and must be integrated at each time step using, for instance, a columnwise implicit method such as the one outlined in reference [1].

Integration Sequence

The system of dynamic equations (5), (14), (22), (23), (24), and the pressure diffusion equation (28) are integrated numerically in small time steps according to the following procedure:

Step 1: Set initial conditions of all degrees of freedom and ψ-distributions for all shoes.

Step 2: Do Steps 3 through 6 for each shoe.

Step 3: Compute clearance distribution and all necessary spatial derivatives. Also check for failure (negative clearance).

Step 4: Integrate pressures to obtain force and torque terms on right-hand side of shoe pitch, roll, and translation equations (22), (23), (24), and contributions to right-hand sides of shaft dynamics equations (5) and (14).

Step 5: Integrate shoe dynamics equations through one time interval.

Step 6: Integrate diffusion equation (28) through one time interval.

Step 7: Sum shoe contributions to total shaft forces and moments.

Step 8: Integrate shaft dynamics equations through one time interval.

Step 9: Has integration proceeded to desired limit? If not, go back to Step 2.

Step 10: Print and plot output; terminate.

Sample Results

Single-Shoe Dynamics

In order to make a simple parametric study of shoe characteristics, the computer program executing the steps indicated in the preceding paragraph can be run so that a single shoe is free to pitch and roll while the shaft is given in prescribed motion. For the cases listed in Table 1, the shaft motion is translatory with a circular orbit. The orbit radius is measured in units of c while the frequency is unity if synchronous with the shaft rotation. The time transient results are shown in Figs. 4 through 15.

A measure of the accuracy of the program is given by comparing a steady-state condition achieved by the dynamic analysis with the results of an equilibrium solution obtained by an entirely different method such as the one presented in reference [1]. Taking the time average values (after the transient has dissipated) for the nondimensional pitch angle Δ and the roll angle Γ, equation (25) can be evaluated to obtain the clearance H. In the single-shoe case

$$A_1 = A_2 = D = X_3' = 0,$$

the pivot is set at $\theta_p = 0$ and, to compute clearances in the plane of the pivot circle, $Z = Z_B$. The leading edge clearance (H_L) can

Table 1 Single-shoe dynamics runs for $R/L = 0.5$; $\alpha = 100$ deg; pivot location, 65 percent; $\rho_{G_2} = D = 0$; pivot friction = 0.

Case	Clear	Shaft-Motion Orbit Radius	Shaft-Motion Orbit Freq.	Λ	Shoe Inertia $I\Gamma$	Shoe Inertia $I\Delta$	Initial Cond. Γ	Initial Cond. Δ
100	1.0	0	0	3.5	26.25	51.95	.2	.2
101	1.0	0	0	3.5	26.25	51.95	.2	-.1
102	.5	0	0	3.5	26.25	51.95	.2	.2
103	1.0	0	0	10	26.25	51.95	.2	.2
104	1.0	0	0	3.5	5.25	10.39	.2	.2
105	1.0	0	0	10	5.25	10.39	.2	.2
106	.5	0	0	10	26.25	51.95	.2	.2
107	.5	0	0	3.5	5.25	10.39	.2	.2
108	.5	0	0	10	5.25	10.39	.2	.2
109	.5	.02	5/9	10	5.25	10.39	.2	.2
110	.5	.10	5/9	10	5.25	10.39	.2	.2
111	.5	.10	1	10	5.25	10.39	.2	.2

Figs. 4 to 15 Single-shoe dynamics results

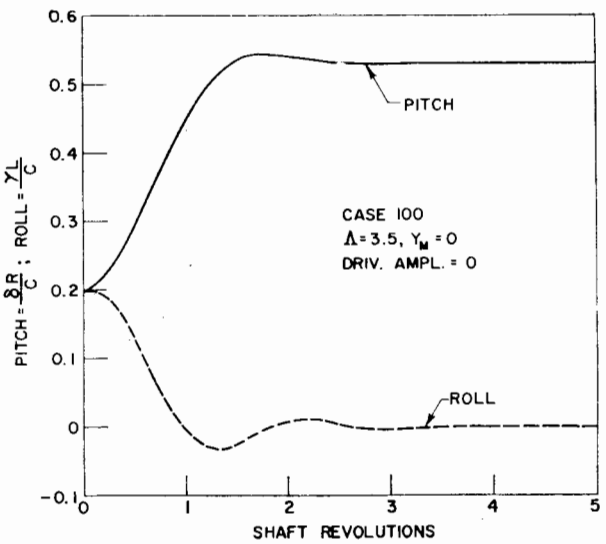

Fig. 4

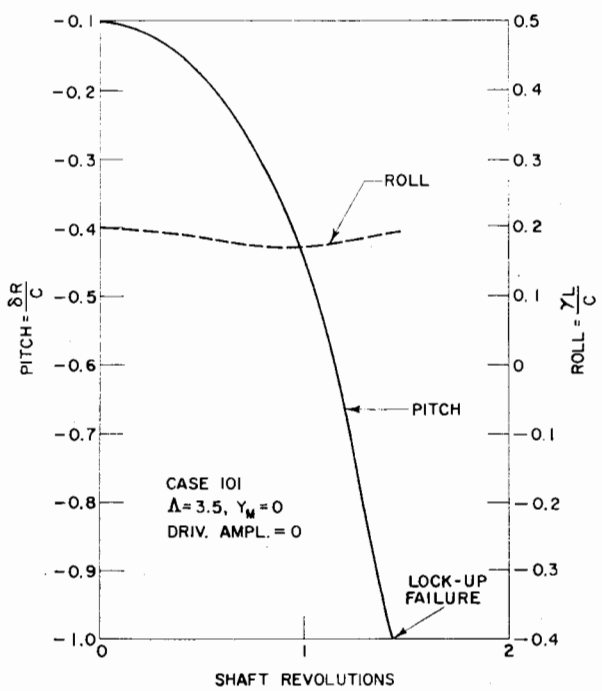

Fig. 5

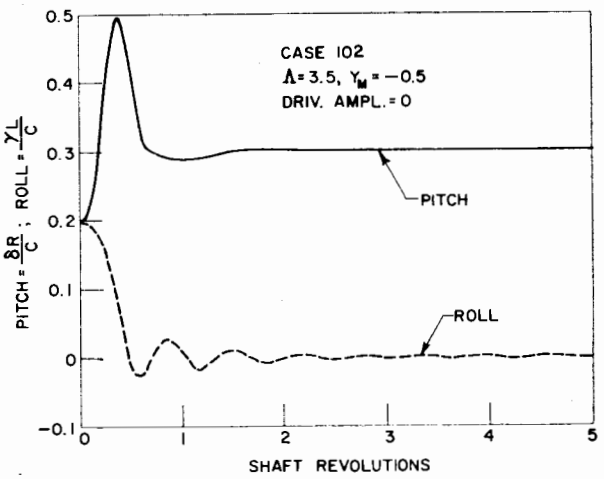

Fig. 6

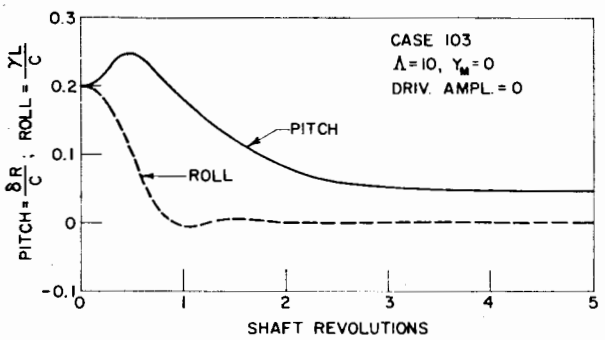

Fig. 7

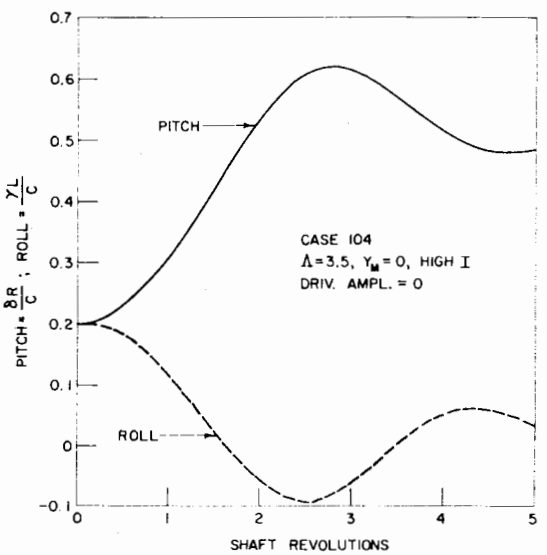

Fig. 8

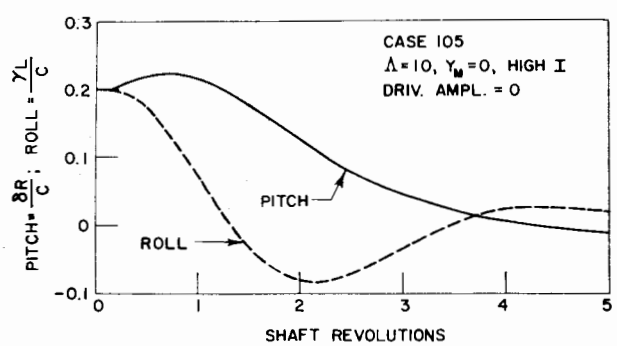

Fig. 9

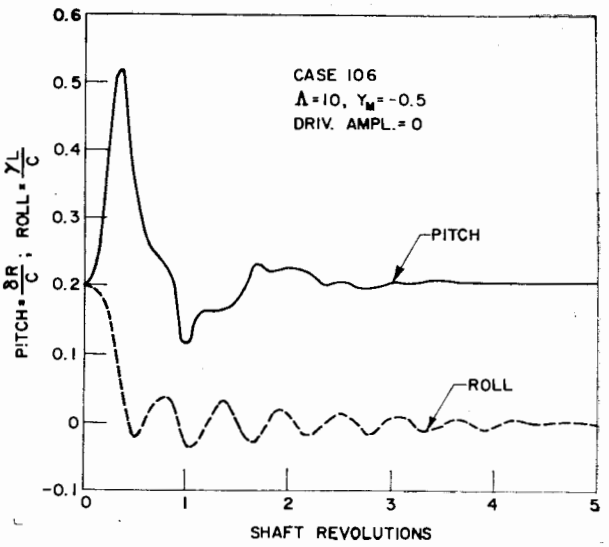

Fig. 10

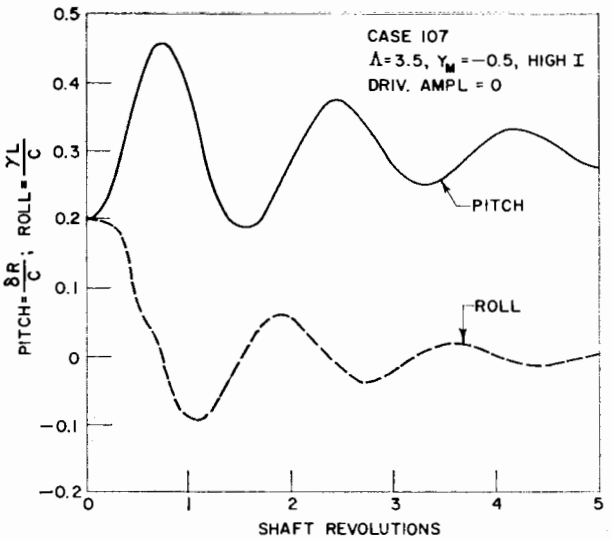

Fig. 11

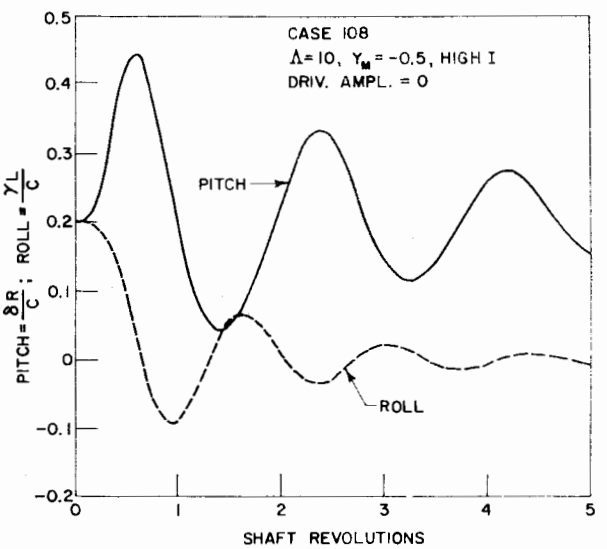

Fig. 12

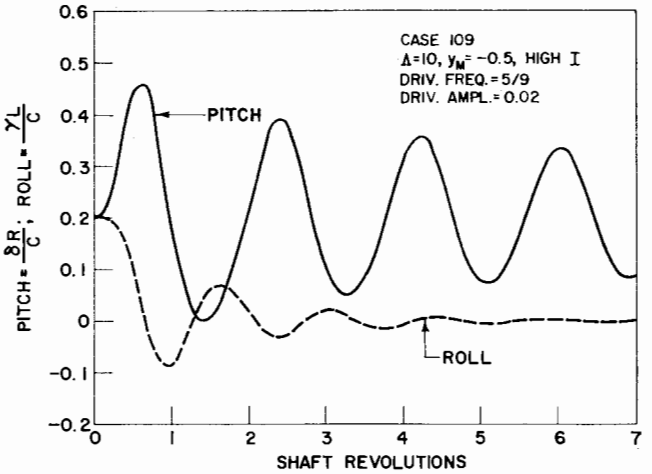

Fig. 13

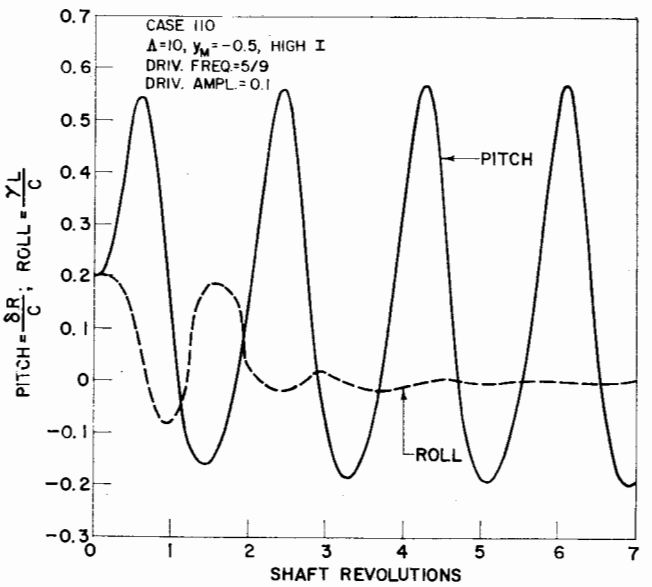

Fig. 14

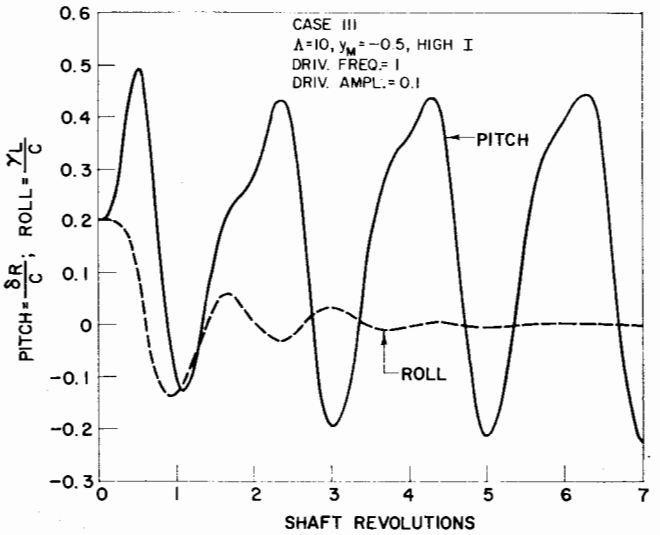

Fig. 15

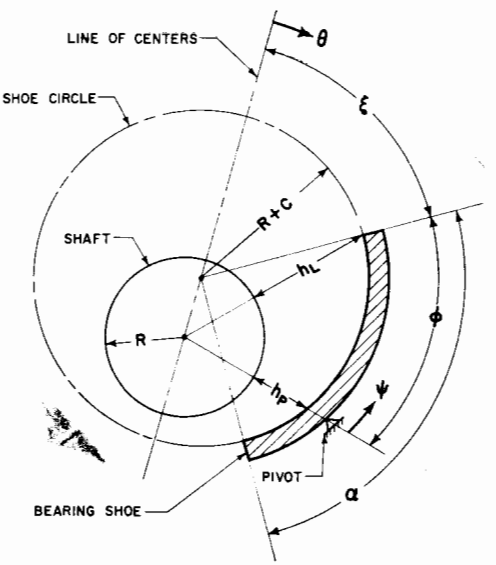

Fig. 16 Shoe-shaft coordinates

be obtained by setting

$$\theta = 2\pi - \phi$$

and

$$\psi = \phi$$

where ϕ is the angle between the shoe leading edge and the pivot point. The pivot film thickness is obtained by setting

$$\theta = \psi = 0$$

Referring to Fig. 16, in terms of the shoe shaft coordinate ($\epsilon = e/c$)

$$H_L = 1 + \epsilon \cos \xi \tag{29}$$

and

$$H_p = 1 + \epsilon \cos (\xi + \phi) \tag{30}$$

Using the values of H_L and H_p obtained by evaluating equation (25), equations (29) and (30) can be used to obtain ϵ and ξ.

The steady-state pivot film thickness for the appropriate parameters is shown in Fig. 17. For $\phi/\alpha = 0.65$ and for a given pivot film thickness, the values of the shoe-shaft coordinates ϵ and ξ can be read from the field map and then compared with those obtained from the dynamic results. Using case 102 ($H_p = 0.5$) for the purpose of comparison, the values of ϵ and ξ resulting from the dynamic analysis are $\xi = 83.2$ deg, $\epsilon = 0.588$, which agree to all accuracy that can be read in Fig. 17 for pivot location = 0.65 and pivot film thickness = 0.5.

Fig. 4 (case 100) represents a "base" case in which the shoe pitch and roll moments of inertia are taken from a typical design application. Note that the shoe is initially pitched open and that it quickly attains an equilibrium position. In case 101 the same conditions as case 100 prevail except that the shoe is initially pitched inward from the uniform clearance position. As can be seen in Fig. 5, the shoe immediately noses into the shaft causing a failure (generally referred to as "lock-up"). Cases 102 and 108 depict the shoe motions which result from changes in Λ, pivot film thickness, and shoe pitch and roll inertia. For the previously mentioned cases the radius of the shaft orbit is zero. The pivot film thickness is given by

$$H_p = 1 + Y_n$$

and the "high I" designation indicates that the shoe inertia (in both pitch and roll) is taken as five times larger than that of the base case. In case 109 and 110 the shaft is given prescribed motions consisting of circular orbits of radius 0.02 and 0.1, respectively, with a frequency corresponding to the pitch motion obtained from case 108. Note that for the larger shaft orbit (case 110) the amplitude seems to be sustained, thereby producing a "flutter" condition.

Case 111 is the same as 110 except that the excitation frequency is made synchronous. In this plot the response is at exactly half frequency with a superimposed synchronous frequency ripple.

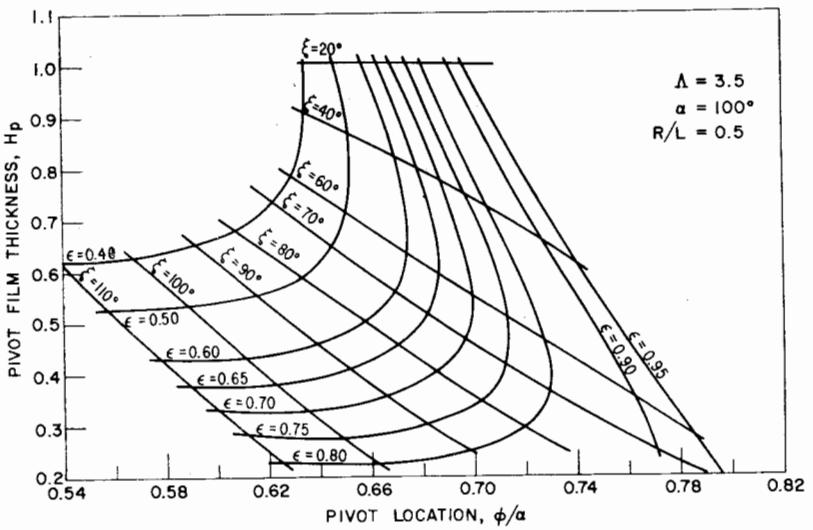

Fig. 17 Pivot film thickness versus pivot location $R/L = 0.5$, $\alpha = 100$ deg, $\Lambda = 3.5$

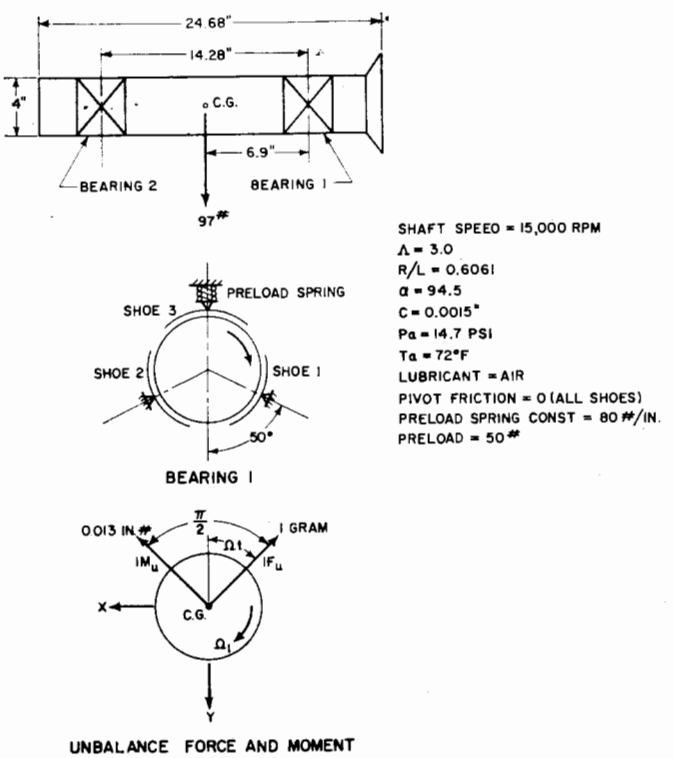

Fig. 18 Rotor-journal bearing system

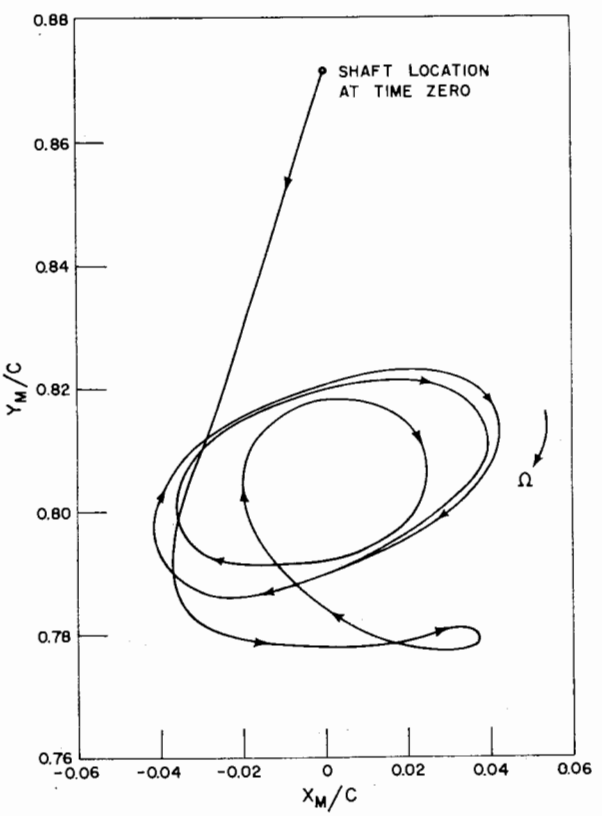

Fig. 19 Transient path of shaft mass center

Multiple Shoe Dynamics

The second system selected for study is the SA-2 gas bearing test rotor, which has been operated at FIRL over the past several years for the purpose of providing experimental information on gas lubricated tilting pad journal bearings (reference [3]). The horizontal rotor is supported by two journal bearings with three pivoted pads each. The top shoe of each bearing is backed by an 80 lb/in. spring (Fig. 18).

Fig. 19 shows the transient path of the shaft mass center starting from an arbitrary initial location. Fig. 20 shows two shaft orbits after the transient has been dissipated; one at the shaft mass center, the other outboard of bearing 1. It can be seen from this figure that the shaft motion displays a significant amount of conical mode. This is due to the relatively high unbalance moment. If the unbalance moment were zero, the two orbits would coincide. Fig. 21 shows the pitch and roll of one of the fixed shoes of bearing 1 while Fig. 22 shows the same motion for the spring-loaded shoe. Note that the pitch amplitude of the fixed shoe is greater than the spring-loaded shoe; also, the roll mode of the fixed shoe displays a superimposed disturbance while the roll of the spring-loaded shoe has a smooth wave form. It is also evident from the shoe motion plots that all pitch and roll frequencies are synchronous.

Not shown in this paper are plots of the x-y coordinates, shaft x-y forces, and the translatory motion of the spring-loaded pivot against time. These plots would show the y-coordinate approximately 180 deg out of phase with the y-force and the spring-loaded pivot about 60 deg out of phase with the y-coordinate.

Validation of the Analysis

Comparison with Steady-State Predictions

A basic check of the dynamical solution procedure is that after a sufficiently long time interval, the time average values of the shoe-shaft coordinates should be those predicted by the steady-state solution. To accomplish this purpose the system selected for analysis was that shown in Fig. 18 with one exception—the

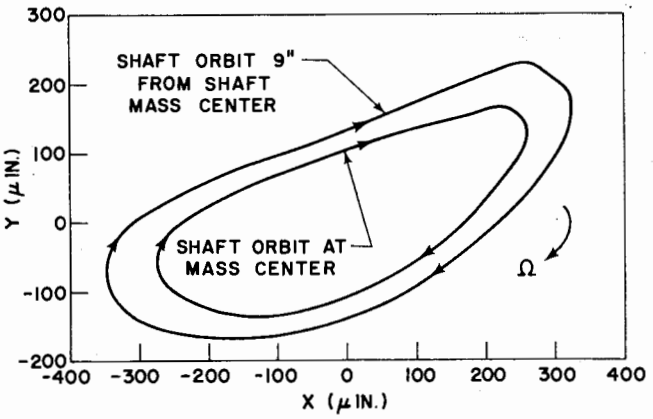

Fig. 20 Shaft orbits—SA-2 rotor

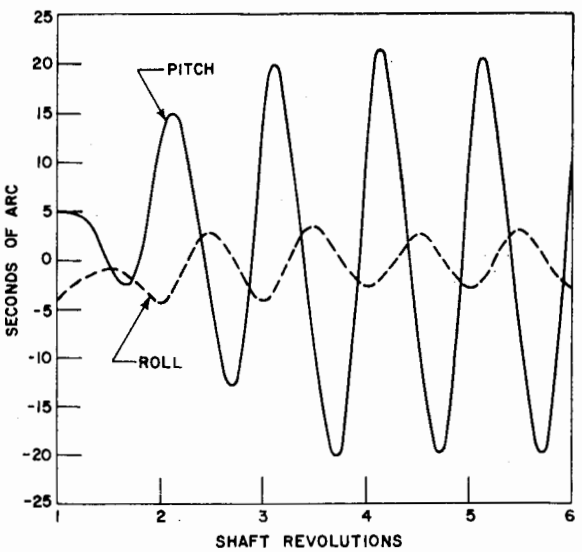

Fig. 21 Pitch and roll motions—bearing 1, shoe 1 SA-2 rotor

unbalance force and moment vectors were taken as zero to cause the shaft orbit to reduce to a point. The appropriate steady-state field maps were used from reference [3] to compute the steady-state coordinates. The percent difference between the dynamical values and the steady-state value is shown in Table 2. The agreement is seen to be excellent. Fig. 23 (reference [4]) shows the degree of agreement that can be expected between the steady-state computed values and experimentally measured values.

Comparison with Experimental Data

Fig. 18 essentially represents the conditions for a particular experimental run made with the SA-2 rig in April, 1964. During this run two capacitance probes measured absolute x-y shaft motion in the same plane; a third probe measured the absolute motion of a fixed shoe; a fourth probe measured the absolute motion of a spring-loaded shoe. Both shoe probes looked at corner-mounted buttons located at the shoe leading edge (Fig. 24).

In formulating the physical data for the dynamics program the following items had to be approximated:

1 The unbalance force was estimated to be 340 milligrams with an uncertainty of ±50 milligrams. The effect of the unbalance force is to change the orbit amplitude.

2 The unbalance moment was known to be small. The estimate of 0.002 in-lb could be in error up to 15 percent. The effect of the unbalance moment is to change the amount of conical motion in the shaft orbit.

3 The machined-in clearance c was taken as 1.5 mils. Due to hand lapping, thermal expansion, and so on, this figure could be in error by ±0.2 mils. The effect of this error would be to change

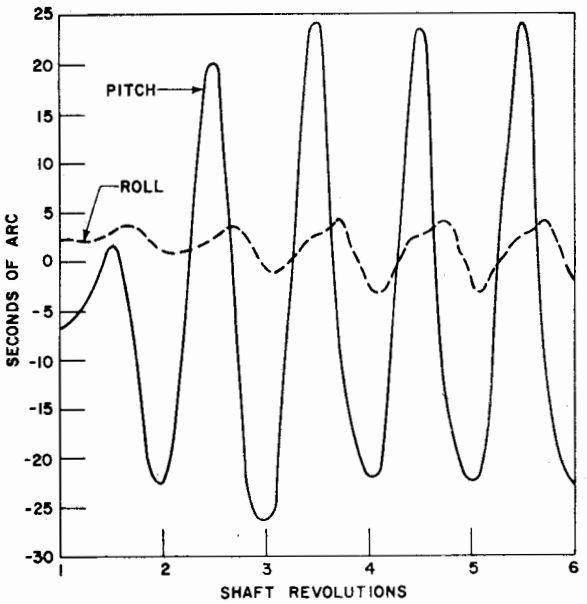

Fig. 22 Pitch and roll motions—bearing 1, shoe 3 SA-2 rotor

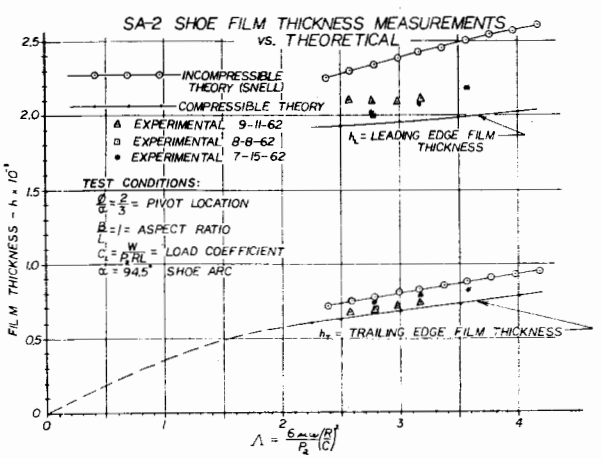

Fig. 23 Comparison between measured and computed values of tilting pad film thickness

Table 2 Validation of time-transient dynamics program

Steady-State Comparison

	Dynamics Program	Steady-State	% Difference
Pivot Film Thickness - shoe 1, 2	0.378	0.38	1/2
Pivot Film Thickness - shoe 3	0.537	0.52	3
Shoe Lead Angle - shoe 1, 2	89.2°	90°	1
Shoe Eccentricity ε - shoe 1, 2	0.69	0.7	1
Shoe Lead Angle - shoe 3	76.1°	77°	1
Shoe Eccentricity ε - shoe 3	0.61	0.63	3
Pivot Circle Preload C'/C	0.431	0.435	1
Pivot Circle Eccentricity ε'	0.176	0.195	10

Λ and thereby alter the shaft pivot circle eccentricity. This would result in a phase change in the shaft orbit due to an apparent change in the ratio of the vertical to horizontal film stiffness.

4 The oscilloscope sweep rate used in determining the shoe motions had an error of 3 percent. The sweep rate for X-Y probes had an error of 10 percent.

5 Other secondary quantities adding to the errors in determining the prevailing conditions during the experimental test run were the shaft speed, the shaft radius, and the ambient pressure.

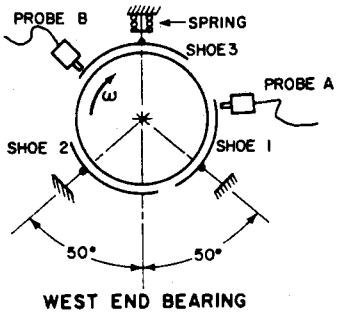

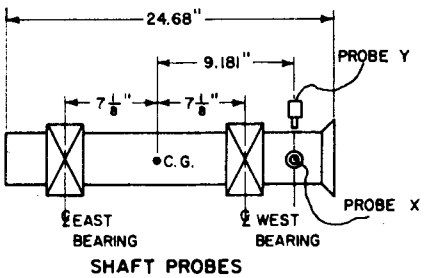

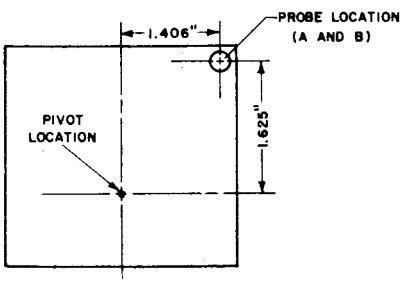

Fig. 24 Instrumentation locations

Table 3 Dynamic comparison

	A_A		A_B		X		Y	
	Comp.	Exp.	Comp.	Exp.	Comp.	Exp.	Comp.	Exp.
Amplitude μin.	245	200	147	280	120	110	60	180
Frequency RPM	15000	15000	15000	15000	15000	13,700	15000	14000

Comp.: computed values; Exp.: experimentally obtained values

Table 3 shows the comparison between the analysis and the experimental data. A_A is the amplitude of shoe number 1 (fixed); A_B is the amplitude of shoe number 3 (spring-loaded). X and Y are the amplitude of the shaft motions in the plane of the probe station. Typical plots of the oscillations of some of the degrees of freedom are shown in Figs. 19 to 22. The experimental oscilloscope photographs corresponding to the various motions measured by the probes are shown in Fig. 25.

To within the known accuracy of the actual experimental operating conditions, the capability of the dynamics program to mimic the experiment is considered good.

Conclusions

In essence, the analysis outlined in the foregoing is similar to making an experimental run. The high degree to which the analysis is capable of mimicking the stability of an actual physical situation makes it an attractive substitute for experimental parametric studies especially since computer time is cheap compared to test rig failures.

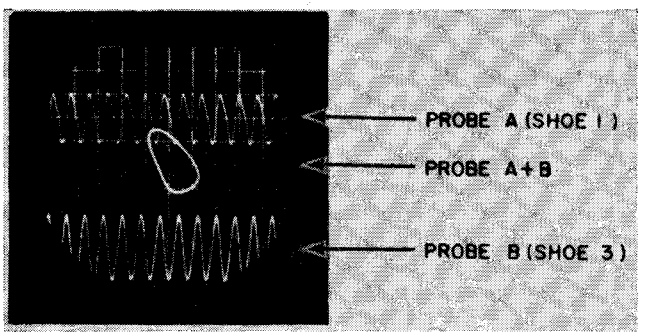

(a) Absolute shoe motion

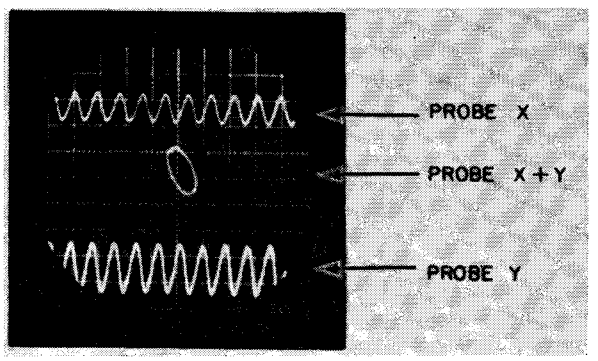

(b) Absolute shaft motion

Fig. 25 Oscilloscope pictures of experimental data used in validation of time-transient dynamics program. Run 4074; shaft speed = 15,000 rpm; scope calibration = 100 μ in./cm; sweep rate = 0.005 sec/cm.

The computer program used in this analysis is currently being updated at the Franklin Institute to include more of the subtle features of the real rotor-bearing physics. The next major step in the development of this program will be the inclusion of the effects of the thrust bearing on the rotor and journal bearing behavior.

Acknowledgment

This work was performed for the Franklin Institute Research Laboratories. The authors would like to thank W. Shugarts and N. Droulard who were instrumental in funding this project.

The validation of the dynamics analysis was made under a NASA subcontract (NAS 3-4179) through Pratt and Whitney Aircraft using experimental and analytical data obtained at FIRL for the U.S. Atomic Energy Commission (references [3] and [4]).

References

1 V. Castelli and J. Pirvics, "Equilibrium Characteristics of Axial Grooved Gas Lubricated Bearings," Columbia University Lub. Research Lab. Report No. 1.

2 V. Castelli and H. G. Elrod, "Solution of the Stability Problem for 360 deg Self-Acting, Gas-Lubricated Bearings," JOURNAL OF BASIC ENGINEERING, TRANS. ASME, Series D, vol. 87, 1965, pp. 199–212.

3 E. J. Gunter, J. G. Hinkle, and D. D. Fuller, "Design Guide for Gas-Lubricated Tilting Pad Journal and Thrust Bearings," Franklin Institute report to U. S. Atomic Energy Commission No. NYO-2512-1, Federal Clearinghouse, November, 1964.

4 E. J. Gunter, J. G. Hinkle, and D. D. Fuller, "The Application of Gas-Lubricated Bearings to High Speed Turbo-Machinery," FIRL Quarterly Technical Report Q-A2392-3-6, June 1, 1962, to August 31, 1962, under AEC Contract No. AT(30-1)-2512.

DISCUSSION

W. J. Love[2]

The tilting-pad, self-acting gas bearing has received increasing recognition by its use as a means of avoiding rotor half frequency whirl. The steady-state performance of tilting-pad bearing arrays has received intensive study in the last decade by means of computer solutions of Reynolds equations. Both authors have provided significant contributions to this work to the point that steady-state design optimization predictions for laminar flow may now be made with confidence.

Tilting-pad, gas-lubricated bearings optimized on a steady-state basis have not been consistently successful in providing stable, noncontacting rotor performance. In some instances the lack of success may be due to lack of detailed knowledge of all of the loads to be exerted on the bearings by the various rotor power conversion components or conditions of rotor unbalance. In many instances, however, the unstable rotor performance has been coupled with a nonsynchronous response of the bearing pads. This nonsynchronous pad response is a phenomenon now evidenced in gas bearings because of the higher rotor speeds and low squeeze film damping associated with gas bearing designs.

While providing a design solution to the rotor half frequency whirl problem, the tilting-pad bearing introduces at least three additional degrees of freedom for each pad, thereby greatly increasing the complexity of an accurate transient analysis of a bearing array. The possibilities for a computer program to examine the dynamics of tilting-pad gas bearings have been recognized for some time, but the amount of machine time indicated has tended to discourage its development.

By circumventing this difficulty, the authors have introduced a very significant analytical tool in the evaluation of the tilting-pad, gas-lubricated bearing. Although the rotor design and journal size for a machine are to a large extent determined by use factors, the effects of the parameters under the control of the bearing designer, i.e., wrap angle, length pivot position, inertia, ground/pivot clearances, and pad damping may now be understood and optimized for their dynamic performance with the program reported in this paper.

The nonsynchronous pad excitation demonstrated in this paper is in substantial agreement with experimental results and observations made in the General Electric Research and Development Center. Last year, a high speed rotor for a regenerative, helium compressor exhibited a double orbit motion of the rotor as full speed ($\sim$ 70 percent of the first rotor bending critical) and full radial load operation was approached. The journals were supported by three identical, self-acting pads mounted symmetrically on rolling contact pivots. It was observed that a condition of $^1/_2$ order subharmonic pitching of the most lightly loaded pads occurred as a precursor of the journal double orbit condition and, if the load or speed were increased beyond this point, pad-journal rubbing would occur. The subharmonic excitation would in many instances appear suddenly as a "jump" change in amplitude and not return to its earlier low amplitude harmonic state without a considerable reduction in speed, load, or the addition of external pad damping. When the rotor load passed between the pivots of two pads, the unloaded pad would exhibit the $^1/_2$ order subharmonic at a lower speed than when the rotor load passed through a pivot. However, when the load passed through a pivot, the rotor double orbit appeared almost simultaneously with the nonsynchronous response of the two lightly loaded pads.

These observations suggested that the rotor orbit instability was caused by the nonsynchronous motion of the pads which in turn had been excited by the rotor orbit and influenced by the pivot film thickness. The $^1/_2$ order subharmonic appeared to be caused by the nonlinear load-displacement characteristic of the gas film.

The equation of motion for pitching of a single pad was derived as a means of providing qualitative understanding of the pad dynamics. The condition of excitation was taken as a harmonic, circular shaft orbit acting at a mean pivot film thickness. The moment characteristics exerted by the gas film upon a pad displaced from its equilibrium condition were generated from steady-state solutions of Reynolds equation similar to those presented in reference [3]. The use of a steady-state moment-angular displacement characteristic neglected the squeeze film damping and force contributions; however, the experimental observations of the film damping indicated that this might be relatively small.

Plotting moment coefficient[3] $C_L\left(\frac{\phi_L}{\alpha}-\frac{\phi_p}{\alpha}\right)$ against a relative pitch coordinate, $\frac{\Delta'}{H_p}\equiv\frac{\epsilon\sin(\xi+\phi_p)}{H_p}$ for various pivot film thicknesses provided curves which could be approximated by parabolas. At intermediate to large pivot film thicknesses the pad restoring moment values were small and, if the nonequilibrium, relative pad-rotor angle became too small, the pad restoring moment would disappear or change sign in a manner to suggest leading edge contact. Indeed, it was found that certain numerical combinations of large pivot film thickness and small pivot angle could not provide an equilibrium operating condition but would provide a moment acting always to cause leading edge pad-rotor contact.

In the case of the aforementioned machine the pitching moment-displacement characteristic was approximated by a parabolic function of the form:[3]

$$C_M = C_L\left(\frac{\phi_L}{\alpha}-\frac{\phi_p}{\alpha}\right)=\frac{m_c}{H_p{}^n}\left[\frac{\Delta'}{H_p}-\frac{Z_1}{H_p{}^u}\right]\left[\frac{\Delta'}{H_p}-\frac{Z_1}{H_p{}^u}+\frac{Z_2}{H_p{}^v}\right]$$

with the equilibrium condition being at $\frac{\Delta'}{H_p}=\frac{Z_1}{H_p{}^u}$

The resulting motion equation form could be compared with the large body of nonlinear oscillation analysis available in the literature.[4] This nonlinear form of the pad moment indicated that the gas film acts as a hard-soft spring—hard at large pitch angles and soft at low pitch angles—the net effect being that of a soft spring. Thus, the resonant frequency of the pad could be expected to be amplitude sensitive, with the resonant frequency becoming smaller than the natural frequency as the amplitude increased; depending upon the degree of damping, the conditions of resonance could occur suddenly as a jump. The essentially parabolic nature of the pad moment characteristic confirmed the potential for a $^1/_2$ order subharmonic pad response to a harmonic rotor excitation. The pitching equation also showed that the natural pitching frequency of the pad, and thus subharmonic threshold frequency, could be increased by increasing the pivot position angle and the ground clearance, and decreasing the pivot film thickness (clearance), rotor orbit size and pad inertia. The pad excitation function occurred as a periodic multiplier of the pad displacement angle and was found to be directly proportional to the rotor orbit and the reciprocal of the mean film thickness. Solutions of the pitching equation for various functions of critical damping showed large amplitude responses at both harmonic and subharmonic resonance with onset of the $^1/_2$ order subharmonic component first becoming perceptible at roughly 120 percent of harmonic resonance. At very high orbit frequencies and large pivot film thicknesses, e.g., when the forcing frequency was greater than three times the natural pad frequency, pad amplitude became very small and of undefined order.

In closing, it is hoped that the authors will be encouraged to examine the pad geometries for typical bearing designs and determine the optimum values of those pad parameters which may

[2] General Engineering Laboratory, General Electric Co., Schenectady, N. Y. Mem. ASME.

[3] The notation is that of reference [3] and the subject paper. Δ prime refers to the relative pitch coordinate and m_c, n, u, v are constants.

[4] N. W. McLachan, *Ordinary Non-Linear Differential Equations in Engineering and Physical Sciences*, Oxford Clarendon Press, London, 1956, chapter IV; or C. Hayashi, *Non-Linear Oscillations in Physical Systems*, McGraw-Hill Book Co., Inc., New York, N. Y., 1964, chapter 7.